Investigation of the $^{14}N(p,\gamma)^{15}O$ reaction and its impact on the CNO cycle

B. Frentz,[1] A. Aprahamian,[1] A. Boeltzig,[1,*] T. Borgwardt,[2,†] A. M. Clark,[1] R. J. deBoer,[1] G. Gilardy,[1] J. Görres,[1] M. Hanhardt,[2,3] S. L. Henderson,[1] K. B. Howard,[1] T. Kadlecek,[2] Q. Liu,[1] K. T. Macon,[1,‡] S. Moylan,[1] C. S. Reingold,[1] D. Robertson,[1] C. Seymour,[1] S. Y. Strauss,[1] F. Strieder,[2] B. Vande Kolk,[1] and M. Wiescher[1]

[1]*Department of Physics and Astronomy and the Joint Institute for Nuclear Astrophysics, University of Notre Dame, Notre Dame, Indiana 46556, USA*

[2]*Department of Physics, South Dakota School of Mines & Technology, Rapid City, South Dakota 57701, USA*

[3]*Sanford Underground Research Facility, Lead, South Dakota 57754, USA*

(Received 28 April 2022; revised 19 September 2022; accepted 15 November 2022; published 20 December 2022)

The CNO cycle is the main energy source in massive stars during their hydrogen burning phase, and, for our sun, it contributes at the ≈1% level. As the $^{14}N(p,\gamma)^{15}O$ reaction is the slowest in the cycle, it determines the CNO energy production rate and thus the CNO contribution to the solar neutrino flux. These CNO neutrinos are produced primarily from the β decay of ^{15}O and, to a lesser extent, from the decay of ^{13}N. Solar CNO neutrinos are challenging to detect, but they can provide independent new information on the metallicity of the solar core. Recently, CNO neutrinos from ^{15}O have been identified for the first time with the Borexino neutrino detector at the INFN Gran Sasso underground laboratory. There are, however, still some considerable uncertainties in the $^{14}N(p,\gamma)^{15}O$ reaction rate under solar temperature conditions. The low energy reaction data presented here, measured at the CASPAR underground accelerator, aim at connecting existing measurements at higher energies and attempts to shed light on the discrepancies between the various data sets, while moving towards a better understanding of the $^{14}N(p,\gamma)^{15}O$ reaction cross section. The present measurements span proton energies between 0.27 and 1.07 MeV, closing a critical gap in the existing data. A multichannel *R*-matrix analysis was performed with the entire new and existing data sets and is used to extrapolate the astrophysical *S* factors of the ground state and the 6.79 MeV transition to low energies. The extrapolations are found to be in agreement with previous work, but find that the discrepancies between measured data and *R*-matrix fits, both past and present, still exist. We examine the possible reasons for these discrepancies and thereby provide recommendations for future studies.

DOI: 10.1103/PhysRevC.106.065803

I. INTRODUCTION

Solar neutrinos are primarily produced by the *pp* chains, which dominate hydrogen burning nucleosynthesis and energy production in our sun [1–3]. The secondary mechanisms for converting hydrogen into helium in the solar environment are the CNO cycles, a catalytic sequence of proton capture reactions, and β decays on C, N, and O isotopes. The primary CNO-I or CN cycle, $^{12}C(p,\gamma)\,^{13}N(\beta^+\nu)\,^{13}C(p,\gamma)\,^{14}N(p,\gamma)\,^{15}O\,^{15}O(\beta^+\nu)\,^{15}N(p,\alpha)\,^{12}C$ [4], is the main source of the CNO neutrinos from the β decay of ^{13}N and ^{15}O isotopes. The CNO cycles contribute ≈1% of solar energy production, but depend critically on the carbon and oxygen abundances of the solar core. An analysis of the CNO neutrino flux, therefore, can provide important information about the metallicity of the core of our sun. The analysis of the neutrino flux, in the context of the reaction cross section of relevance here, requires detailed knowledge of all the associated reaction rates.

In the standard solar model [5,6], one of the major uncertainties in the description of the sun's interior is the metallicity of the core, which is determined by its carbon, nitrogen, and oxygen content [7]. The expected elemental abundances, based on the spectroscopic analysis of the solar atmosphere, disagree with the solar profiles of sound speed and density as well as the depth of the convective zone and the helium abundance obtained by helioseismology [1]. Haxton and Serenelli [8] noted that a direct study of the CN neutrinos, those from the β decay of ^{13}N and ^{15}O, can provide an independent measure of the solar metallicity. However, the CN neutrino flux depends not only on the CN abundance in the solar interior, but also on the associated CN reaction rates, $^{12}C(p,\gamma)\,^{13}N$ and $^{14}N(p,\gamma)\,^{15}O$, respectively, since the CN neutrino flux originates from the β decays of ^{13}N and ^{15}O. The $^{14}N(p,\gamma)^{15}O$ reaction is the slowest process in the cycle, thus its rate limits the energy release and neutrino production of the entire cycle. The slow rate causes a gradual enrichment of ^{14}N in the solar material. This, and the shorter lifetime of

*Present address: Helmholtz-Zentrum Dresden-Rossendorf (HZDR), 01328 Dresden, Germany.

†Present address: Los Alamos National Laboratory, Los Alamos, NM 87545, USA.

‡Present address: InstroTek Inc., 1 Triangle Drive, PO Box 13944, Research Triangle Park, NC 27709, USA.

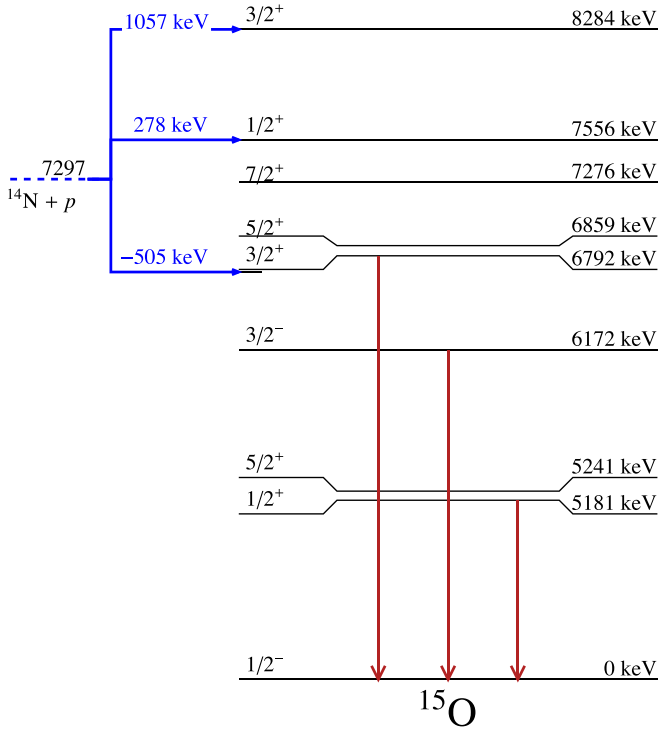

FIG. 1. Level scheme of the ^{15}O compound nucleus. The resonance (laboratory frame) energies and corresponding excitation energies of the pertinent states are given. As noted, the transitions to the 6.79 MeV state and ground state are two of the strongest, and are the transitions reported in this work. All of the states at or below the 6.79 MeV level de-excite with nearly 100% branching to the ground state.

^{15}O in comparison to the lifetime of ^{13}N, suggests that CNO neutrinos will be dominated by the β decay of ^{15}O.

The first comprehensive study of the individual partial cross sections of the ^{14}N$(p,\gamma)^{15}$O reaction was performed by Schröder *et al.* [9], who reported both excitation functions and angular distributions at select energies, covering the proton energy range from $E_p = 0.2$ to 3.6 MeV. The total S factor at zero energy, $S(0)$, was determined to be 3.20 ± 0.54 keV b, where the transitions to the ground state and to the $E_x = 6.79$ MeV excited state in ^{15}O were reported to be dominant, contributing $S_{\text{g.s.}}(0) = 1.55 \pm 0.34$ keV b and $S_{6.79}(0) = 1.41 \pm 0.02$ keV b to the total, respectively. Figure 1 depicts the relevant level structure of the ^{15}O compound nucleus near the proton separation energy, including these two important states.

An R-matrix analysis by Angulo and Descouvemont [10] drastically changed the extrapolated S factor for both transitions after realizing that the data from Schröder *et al.* [9] were yields and not cross sections. They revised the S factors to $S_{\text{g.s.}}(0) = 0.08^{+0.13}_{-0.06}$ keV b and $S_{6.79}(0) = 1.63 \pm 0.17$ keV b. Overall, this reduced the total S factor by a factor of 1.7. A number of more recent measurements at the LUNA underground accelerator [11–14] expanded the reaction data to lower energies, suggesting an even lower S factor, while an independent study by Runkle *et al.* [15], at the LENA facility, indicated a higher value for the ground state transition. The reported S factors, extrapolated to zero energy, from different measurements are summarized in Table I.

An independent R-matrix analysis of the various reaction channels, over a wide range of energies by Azuma *et al.* [19], incorporating more data sets, found results in agreement with Imbriani *et al.* [11], although with a slightly higher zero-energy S factor for the ground state transition of $S_{\text{g.s.}}(0) = 0.28$ keV b. The authors stated that there was still considerable uncertainty, most notably contributions from the resonances above 2 MeV, the low-energy ground state transition data, and the width of the 6.79 MeV subthreshold state. A modified version of this R-matrix fit, which focused on the low energy region, was used for the evaluation of Adelberger *et al.* [3].

Daigle *et al.* [22] provided a new measurement and evaluation of the branching ratios and strength of the $E_p = 278$ keV resonance, finding a value for the strength of 12.6 ± 0.3 meV. This result is significantly more precise than previous measurements, providing an improved normalization for the data. It is also worth pointing out that when this value for the strength is used to normalize all of the data, they then share a common systematic uncertainty in their normalizations. This must be considered in global fits and in the propagation of the uncertainties from them.

Li *et al.* [20] sought to better constrain the several different reaction contributions to the low energy cross section. They, for the first time, measured differential cross sections, at up to five angles, over the proton energy range between 1.5–3.4 MeV for the 6.79 MeV transition, and from 0.6–3.4 MeV for the ground state transition. They also realized that an error had been made in the R-matrix fits of both Azuma *et al.* [19] and the evaluation of Adelberger *et al.* [3], where the $\ell = 2$ terms in the calculation had been neglected. However, its inclusion led to a poorer representation of the experimental data, and a consistent fit covering their higher energy range data and the lower energy measurements of Imbriani *et al.* [11] could not be achieved. For their extrapolated S factors, the authors reported $S_{6.79}(0) = 1.29 \pm 0.04(\text{stat}) \pm 0.09(\text{syst})$ keV b and $S_{\text{g.s.}}(0) = 0.42 \pm 0.04(\text{stat})^{+0.09}_{-0.19}(\text{syst})$ keV b. The authors identified the primary remaining sources of uncertainty as the γ width of the 6.79 MeV state in ^{15}O, the ground state and the 6.17 MeV transition. Critically, the data reported do not overlap with the low energy measurements of the LUNA and LENA groups, contributing to the difficulty in achieving a consistent R-matrix fit.

Wagner *et al.* [21] followed up on these results by attempting to bridge the gap between the higher energy data sets of Li *et al.* [20] and Schröder *et al.* [9] and the low energy data. They focused on the cross section for the transition to the 6.79 MeV state and ground state at proton energies between 0.36 and 1.29 MeV. Their reported values for the S factors are $S(0)_{\text{g.s.}} = 0.19 \pm 0.05$ keV b and $S(0)_{6.79} = 1.24 \pm 0.11$ keV b. For the 6.79 MeV transition, particularly above $E_p = 0.8$ MeV, they found cross sections significantly elevated compared to those of either Schröder *et al.* [9] or Li *et al.* [20]. The authors note that, following these analyses, there are still sources of significant uncertainty in the reaction data.

New measurements have also been made of the γ width of the 6.79 MeV subthreshold state in ^{15}O by Frentz *et al.* [23], following several previous studies [24–29]. As noted in

TABLE I. A summary of zero energy S factors for the $^{14}N(p,\gamma)^{15}O$ reaction.

		Astrophysical S factor $S(0)$ (keV b)				
Year	Reference	R/DC → 0.00	R/DC → 6.792	R/DC → 6.172	Others[d]	Total
1987	Schröder *et al.* [9]	1.55 ± 0.34	1.41 ± 0.02	0.14 ± 0.05	0.1	3.20 ± 0.54
2001	Angulo *et al.*[a] [10]	$0.08^{+0.13}_{-0.06}$	1.63 ± 0.17	$0.06^{+0.01}_{-0.02}$	––	1.77 ± 0.20
2003	Mukhamedzhanov *et al.* [16]	0.15 ± 0.07	1.40 ± 0.20	0.133 ± 0.02	0.02	1.70 ± 0.22
2004	Formicola *et al.* [17]	0.25 ± 0.06	1.35 ± 0.05 (stat) ± 0.08 (sys)	$0.06^{+0.01}_{-0.02}$[b]	0.04	1.7 ± 0.1 (stat) ± 0.02 (sys)
2005	Imbriani *et al.* [11]	0.25 ± 0.06	1.21 ± 0.05	0.08 ± 0.03	0.07	1.61 ± 0.08
2005	Runkle *et al.* [15]	0.49 ± 0.08	1.15 ± 0.05	0.04 ± 0.01	––	1.68 ± 0.09
2005	Angulo *et al.* [18]	0.25 ± 0.08	1.35 ± 0.04	0.06 ± 0.02	0.04	1.70 ± 0.07 (stat) ± 0.10 (sys)
2006	Bemmerer *et al.* [13]	––	––	––	––	1.74 ± 0.14 (stat) ± 0.14 (sys)[c]
2008	Marta *et al.* [14]	0.20 ± 0.05	––	0.09 ± 0.07	––	1.57 ± 0.13
2010	Azuma *et al.* [19]	0.28	1.3	0.12	0.11	1.81
2011	Adelberger *et al.* [3]	0.27 ± 0.05	1.18 ± 0.05	0.13 ± 0.06	0.08	1.66 ± 0.08
2016	Li *et al.* [20]	0.42 ± 0.04 (stat) $^{+0.09}_{-0.19}$(sys)	1.29 ± 0.06 (stat) ± 0.06 (sys)	––	––	––
2018	Wagner *et al.* [21]	0.19 ± 0.01 (stat) ± 0.05 (sys)	1.24 ± 0.02 (stat) ± 0.11 (sys)	––	––	––
2022	This work	$0.33^{+0.16}_{-0.08}$	1.24 ± 0.09	0.12 ± 0.04	––	1.69 ± 0.13

[a] R-matrix analysis on available data, not a measurement.
[b] Adopted from Angulo and Descouvemont [10].
[c] Measured S factor at 70 keV.
[d] Calculated difference of the total $S(0)$ from the other transitions.

the analyses of Li *et al.* [20] and Adelberger *et al.* [3], this component was one of the largest source of uncertainty in the low-energy extrapolations of the cross section. The work by Frentz *et al.* [23] found a lifetime of $\tau = 0.6 \pm 0.4$ fs, placing the most stringent limit on the lifetime to date, and, therefore, the width of the state. These results, however, when combined with an R-matrix analysis, demonstrated that the uncertainty in the lifetime still remains too large to significantly reduce the uncertainty in the extrapolation of the low energy S factor.

On the neutrino side, the Borexino collaboration has succeeded in the first measurement of the CNO neutrinos associated primarily with the β decay of ^{15}O in our sun [30]. Their results suggest an enhanced reaction rate, and therefore a larger cross section, for the $^{14}N(p,\gamma)^{15}O$ reaction at low energies. The suggested cross section is more in line with the higher low-energy extrapolation based on the LENA data [15] rather than that obtained using the LUNA data [11–14]. The low energy extrapolation by Li *et al.* [20] utilized a more comprehensive R-matrix analysis, covering a wide energy and angular range. Their extrapolation was also found to be inconsistent with the low energy data of Imbriani *et al.* [11], yet consistent with the data of Runkle *et al.* [15].

In light of these existing discrepancies, and those in the higher energy data presented by Wagner *et al.* [21], a new measurement of the $^{14}N(p,\gamma)^{15}O$ reaction cross section has been performed. In particular, the energy range targeted in this work bridged the gap between the low energy data of LUNA [11–14] and LENA [15] and the high energy data of Li *et al.* [20], in order to work towards a consistent R-matrix analysis that includes the entire data ensemble. The ground state and the 6.79 MeV transition are therefore the main focus.

In this work, we report on a measurement, providing a new and independent cross section for two of the most important transitions in the $^{14}N(p,\gamma)^{15}O$ reaction, namely the transitions to the ground state and the 6.79 MeV level with proton energies between 0.27 and 1.07 MeV. The experimental details are first discussed in Sec. II, covering the setup and measurement. In Sec. III, the data analysis is explained and the cross sections are presented. R-matrix calculations incorporating the new data from this measurement and the corresponding reaction rate calculations are described in Secs. IV and VI, respectively. Section V contain discussions of the results and their implications for the flux of CNO neutrinos. Finally, the summary and conclusions are presented in Sec. VII.

II. EXPERIMENTAL METHODOLOGY

A. Accelerators and setup

The measurements were performed using the 1 MV JN Van de Graaff accelerator located at the Compact Accelerator System for Performing Astrophysical Research (CASPAR) [31] at the Sanford Underground Research Facility [32]. The primary advantage of the CASPAR facility is the low-background environment. Located nearly a mile underground in the Black Hills of South Dakota, the rock overburden (4300 mwe) between the CASPAR facility and Earth's surface shields from cosmic rays, decreasing the high energy

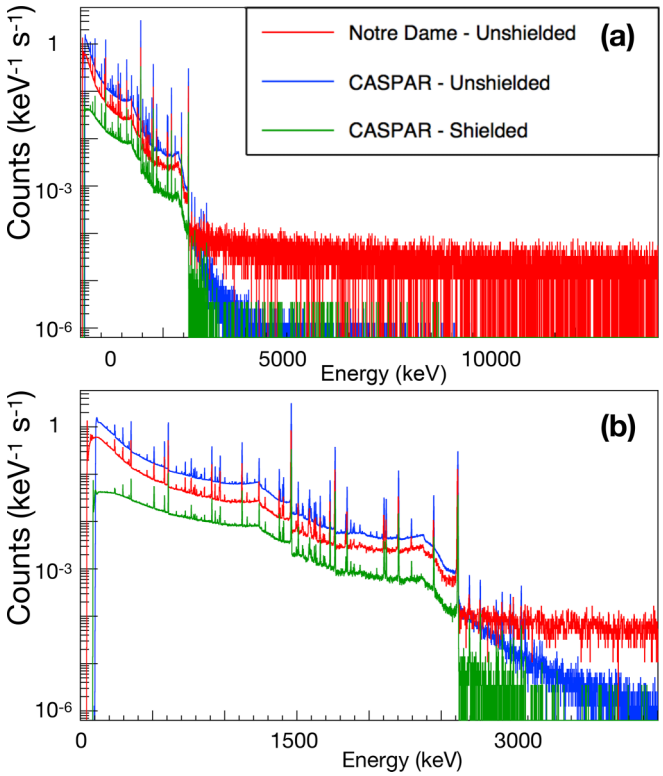

FIG. 2. Background γ-ray spectrum taken at the deep underground CASPAR facility (with and without lead shielding) and the Notre Dame Nuclear Science Laboratory (a surface laboratory). (a) The full spectrum. (b) The low-energy subset of the spectrum highlighting the radiogenic background region, which is higher at the CASPAR facility when lead shielding is not employed, because of decays from the surrounding rock.

background from γ rays by orders of magnitude. Further, in this environment, lead shielding is even more effective, reducing low energy γ rays from room background without producing additional ones from cosmic ray interactions with the lead itself. This dramatic background reduction is shown in Fig. 2.

Proton beams from laboratory energies $E_p = 0.27$ to 1.07 MeV were produced from the 1 MV JN accelerator with typical intensities between 50 and 100 μA on target. The energy calibration of the machine was established to better than 1 keV, using the well-known $^{27}\mathrm{Al}(p,\gamma)^{28}\mathrm{Si}$ resonance at 992 keV [33] and the $^{14}\mathrm{N}(p,\gamma)^{15}\mathrm{O}$ resonance at 278 keV [34].

Targets were mounted on a 45° target holder, relative to the beam axis and, due to the high beam currents, the backings were constantly cooled with recirculating deionized water. A copper cold finger, biased to −400 V and cooled with a liquid nitrogen reservoir, was utilized to limit carbon build-up and suppress secondary electrons throughout the measurements. The position of the beam on the target was defined by pairs of vertical and horizontal slits to prevent drifting on the face of the targets throughout the course of the runs.

B. Targets

The ZrN targets were fabricated at the Karlsruhe Nano Micro Facility by reactive sputtering of Zr in a nitrogen atmosphere enriched in $^{14}\mathrm{N}$ to >99.99% in two batches to nominal thicknesses of 50 and 100 nm, respectively. The thicknesses the three targets used in this experiment were measured using the narrow resonance at $E_p = 278$ keV in the $^{14}\mathrm{N}(p,\gamma)^{15}\mathrm{O}$ reaction and were found to produce proton beam energy losses of 11.2 ± 0.2 keV, 11.5 ± 0.1 keV, and 20.8 ± 0.1 keV. The stability of these targets was also continuously monitored during the course of the experiment by remeasuring this resonance and monitoring the target profile. Target degradation, as shown in Fig. 3, was found to be linearly dependent on the integrated charge.

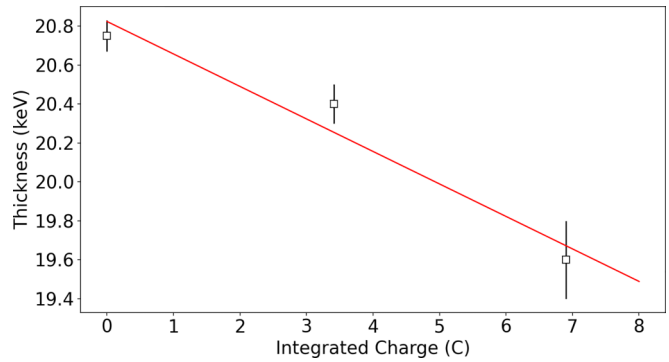

FIG. 3. Typical deterioration of the ZrN targets used in this experiment. The thickness was measured by scanning the $E_p = 278$ keV resonance in the $^{14}\mathrm{N}(p,\gamma)^{15}\mathrm{O}$ reaction. This degradation was used to correct for the amount of nitrogen in the target.

C. γ-ray detector

De-exciting γ rays were observed with a Canberra coaxial p-type high-purity germanium (HPGe) detector, of 130% relative efficiency. A lead sheet, of 1.5 mm thickness, was placed between the crystal's face and the target to attenuate low-energy x rays, greatly reducing the count rate from low energy beam induced reactions. Lead bricks were placed around the detector, at least 10 cm thickness on all sides, in order to reduce the radiogenic background from uranium and thorium decay chains in the rock environment surrounding the experimental hall. The detector was placed at 55° relative to the beam axis to minimize angular distribution effects, as shown schematically in Fig. 4. Additionally, the detector was on an adjustable table, allowing it, and the lead shielding, to be moved closer or further from the target. This was necessary in order to reduce the high count rate during some of the runs. At the closest distance, the detector face was 1.0 cm away from the target and 25.4 cm away from the target at the furthest geometry. The table's guide rails also contained block stops, making the detector's distance to target reproducible in each position. All of the data used for the cross section measurements were obtained at the 1.0 cm distance.

III. ANALYSIS AND RESULTS

A. Efficiency and summing

The full-energy peak HPGe detector efficiency was measured using transitions from the well-known $E_p = 278$ keV

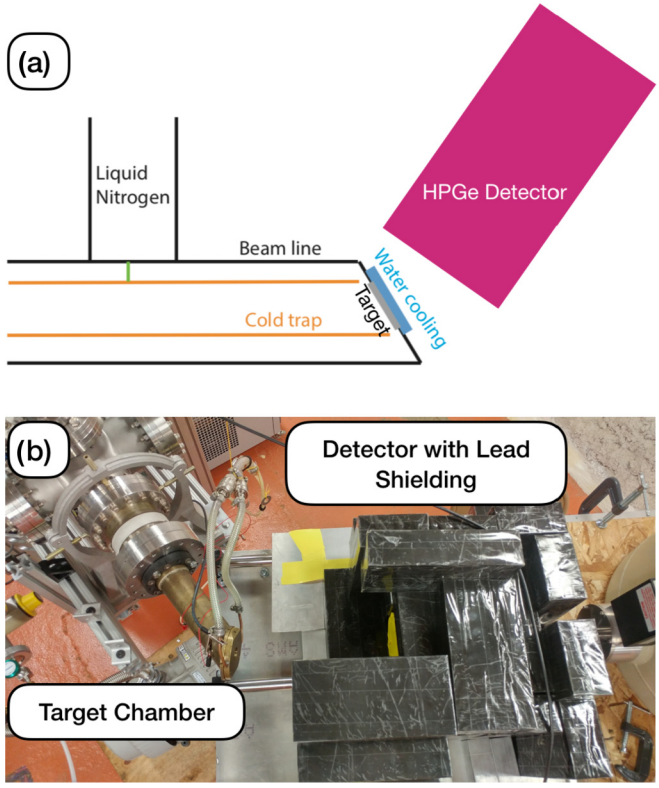

FIG. 4. (a) Schematic of the experimental setup. For clarity, the lead shielding that surrounded the detector during the measurement is not shown. (b) Overhead picture of the experimental setup showing the detector and lead shielding in the far distance configuration.

resonance in the ^{14}N$(p,\gamma)^{15}$O reaction [22]. A polynomial function of third order was used to fit the full-energy-peak (FEP) efficiency [35]

$$\epsilon(E_\gamma) = \exp\left(\sum_{i=0}^{n} a_i \ln(E_\gamma)^i\right), \tag{1}$$

where a_i are fit parameters and E_γ is the γ-ray energy.

As noted in Sec. II C, the entire detector setup could be moved to different distances from the target and the data were taken in both near and far geometries. At near distances, the count rate was high and summing effects were significant, whereas the count rate was low and there was negligible summing at far distance. We therefore determined the relative efficiencies at far distance, in the absence of summing, and scaled the efficiency curve for the near distance, where the data in the experiment were measured. The scaling was determined using the monoenergetic, isotropic, 2365 keV decay from the ^{12}C$(p,\gamma)^{13}$N reaction on top of the 450 keV resonance. The ratio of counts measured in the near/far distances from this additional reaction directly provides the relationship necessary to scale the far-distance fitted efficiency curve. The efficiency curves are shown in Fig. 5, where we note that the close distance efficiency curve is not a fit to the data, but is the efficiency determined from the far distance configuration scaled by the correction ratio obtained from the ^{12}C$(p,\gamma)^{13}$N reaction.

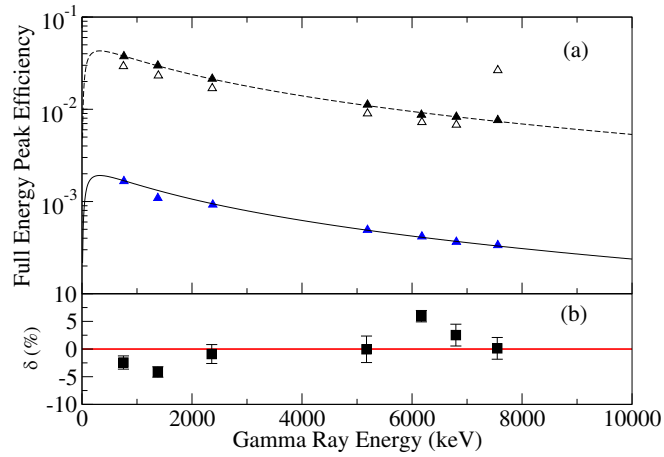

FIG. 5. Efficiency calibration of the 130% HPGe placed at 55° relative to the beam axis. (a) Full-energy peak efficiency for a single γ ray as a function of γ-ray energy and detector setup. The two setups had the detector placed 1.0 and 25.4 cm away from the target. The open markers are efficiencies uncorrected for summing effects while the full markers include them. The line through the far distance points was fit to the data while the line for the near distance was scaled by the difference in solid angle subtended by the detector in the two distances. (b) Relative residuals (δ) between the corrected data and the efficiency curve at the detector distance of 1.0 cm.

Broadly speaking, summing effects arise when multiple photons deposit a portion or all of their energy in the detector at the same time. When this occurs, the individual γ-ray peaks have fewer counts (summing-out) and artificial counts are added at their energy sum (summing-in). With large detection efficiencies or small distances between the detector and source, the effect of the coincidence summing was significant and had to be taken into account. The summing effects can be observed directly in the uncorrected, close distance efficiency data present in Fig. 5 (open triangles), where the summing-out effect decreases the primary and secondary counts for each of the three transition cascades, while the summing-in effect causes the ground state counts to be increased.

For a primary/secondary pair of decays in a cascade, the summing-out effects can be determined with

$$Y_i^{\text{pri}} = RB_i\eta^{\text{FEP}}\left(E_\gamma^{\text{pri}}\right)\left(1-\eta^{\text{TOT}}\left(E_\gamma^{\text{sec}}\right)\right), \tag{2}$$

$$Y_i^{\text{sec}} = RB_i\eta^{\text{FEP}}\left(E_\gamma^{\text{sec}}\right)\left(1-\eta^{\text{TOT}}\left(E_\gamma^{\text{pri}}\right)\right), \tag{3}$$

where i denotes a specific transition sequence, Y_i represents the measured yields of the primary and secondary (pri/sec) transitions, R is the number of reactions per incoming particle, B_i are the branching ratios for the respective transitions, and η^{FEP} and η^{TOT} are the full-energy peak and total efficiencies, respectively [35,36]. Note that in the case of the primary transition, specifically, the summing-out correction is constant regardless of the reaction's incident proton energy because the secondary transition itself has a fixed γ-decay energy. For this reason, in this analysis we only considered data from the primary decays for the nonground state transitions. Using the same close/far distance ratios determined by the use of the ^{12}C$(p,\gamma)^{13}$N reaction described above, the summing-out

TABLE II. Geometric Q coefficients.

Q_1	0.92
Q_2	0.90
Q_3	0.87
Q_4	0.82

corrections for each of the transitions can be determined on top of the $E_p = 278$ keV resonance by comparing the expected amount (determined again from the scaled efficiencies) with the observed peak counts. Thus, determining these summing-out corrections for the resonance data allowed us to apply summing-out corrections for all data taken in the experiment.

Armed with the summing-out corrections and the efficiencies, the summing-in contribution is straightforward to obtain. For the nonground state transitions in the $^{14}\mathrm{N}(p,\gamma)^{15}\mathrm{O}$ reaction, the decays proceed through a series of two-step cascades, where every secondary transition has a 100% branching ratio to the ground state, (see Fig. 1), and each of their sum contributions will match exactly with the ground state transition. Mathematically, for a single cascade pair, the contribution of this cascade to the full sum-peak can be written as

$$Y_{\mathrm{sum}}\left(E_\gamma^{\mathrm{pri}} + E_\gamma^{\mathrm{sec}}\right) = RB_i\eta^{\mathrm{FEP}}\left(E_\gamma^{\mathrm{pri}}\right)\eta^{\mathrm{FEP}}\left(E_\gamma^{\mathrm{sec}}\right), \qquad (4)$$

because this contribution is the case where the full energy of both transitions are deposited at the same time and the resultant sum-peak's energy matches the ground state transition. Therefore, to correct for the summing-in effects, we took the product of the full-energy photopeak efficiencies with the summing corrected counts in the primary peak for all of the transitions. As the summing correction is dependent on the cross-section of the other contributing transitions, the correction is not constant (it is, however, well studied [11]); for the nonresonant ground state transition data, the summing contribution was dominated by the 6.79 MeV transition cascade, and the average correction was 54%. The summing-in effects on the ground state transition are clear in Fig. 5 (open triangles), as is the accuracy of the summing correction to this data (closed triangles). As discussed above, the measurements were taken at the different distances between the detector and target (1.0 cm and 25.4 cm), moving the detector stand on rails to ensure the detector remained on the same 55° axis relative to the beam. These different distance measurements allowed for the characterization and correction of the summing effects in order to produce the efficiency curves shown in Fig. 5. All measured yields in close measurement geometry were corrected for summing effects, as can also be seen in the near data of Fig. 5. The measurements at different distances were also used to determine the geometric Q coefficients [37] of the setup (see Table II).

B. Spectrum analysis and fitting procedures

A typical spectrum, taken with the HPGe detector in the high-energy region, is presented in Fig. 6. The spectrum shows a strong population of the 6.79 MeV and 6.17 MeV states through their secondary γ-ray decays to the ground state. The primary γ-ray peak of the ground state transition is also visible.

The well-known contamination line at 6.13 MeV was observed in spectra taken above $E_p = 340$ keV, which originates from fluorine in the target backings via the $^{19}\mathrm{F}(p,\alpha\gamma)^{16}\mathrm{O}$ reaction. This peak includes a wide, Doppler-broadened component underneath a sharp Gaussian peak, which overlaps the secondary transition of the 6.17 MeV excited state. This fact, alongside the relatively weak population of this state at many energies, is the reason no analysis of this transition is attempted in this work or those of many others.

In fitting the peaks present in the spectra, the centroid, area, and width are determined directly from the bin contents in the histogram. By simply dealing directly with the bin contents, the fitting is blind to any shape variation in the peak, which can influence the area determined from more complicated fits. The net areas of the peaks were found after subtracting a background contribution from the surrounding spectrum, determined by a cubic fit of equivalent regions surrounding the peak of interest. In the high-energy region of the spectrum, where we are concerned, a cubic background is a reasonable assumption, as the background is small and the peaks of interest are typically well isolated from each other. Often, the cubic term and quadratic terms were consistent with zero, simplifying to a linear background.

C. Cross section determination

The excitation function for the transition to the 6.79 MeV and ground state for the $^{14}\mathrm{N}(p,\gamma)^{15}\mathrm{O}$ reaction have

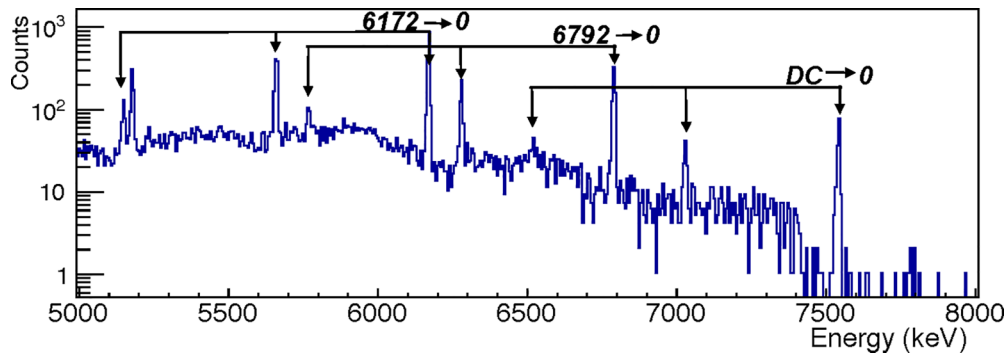

FIG. 6. A typical example of the high-energy part of the γ-ray spectrum obtained in this experiment. Specifically, the data taken at $E_p = 270$ keV, with the detector in close geometry, and approximately 1 C of integrated charge during this run.

TABLE III. Summary of systematic uncertainty estimates.

Systematic uncertainty contribution	%
Charge collection	3
Stopping power	5
Efficiency	5
278 keV resonance strength	2.4
Branching ratio (g.s./6.79)	2/1.3
Total	8.3

been measured over the proton energy range from 0.27 to 1.07 MeV. The experimentally observed yields $Y(E_p)$ were found by correcting the peak areas for the delivered charge, target degradation, detector efficiency, and summing effects. For each of the transitions analyzed here, the primary γ rays were used to experimentally determine the yield. The differential cross sections were calculated from these yields via

$$\frac{d\sigma(E)}{d\Omega} = \left(\frac{\lambda_R^2}{2}\right)\frac{\omega\gamma B_i}{\Delta(E_p)}\frac{Y(E)}{Y_{\max}(\infty)}, \tag{5}$$

where λ_R is the de Broglie wavelength of the system, the resonance strength $\omega\gamma = 12.6 \pm 0.3$ meV and B_i, the branching ratio for a given transition, were obtained from [22], $\Delta(E_p)$ is the target thickness specific to the individual data point at the incident beam energy, E_p, $Y(E)$ is the yield for a given data point, and $Y_{\max}(\infty)$ is the thick target yield on the resonance. The point-to-point uncertainty contributions come from statistics and target stability, while the remaining uncertainties are treated as common-mode systematic uncertainties and are summarized in Table III. The resulting differential cross sections and S factors obtained in this work are shown in Figs. 7–10. The S factors were calculated using the AZURE2 code [19], as described in Sec. IV. The data are provided in the Supplemental Material [38].

IV. *R*-MATRIX ANALYSIS

An R-matrix analysis, using the AZURE2 code [19,40], was used to simultaneously fit the ground state, $E_x = 6.17$ and

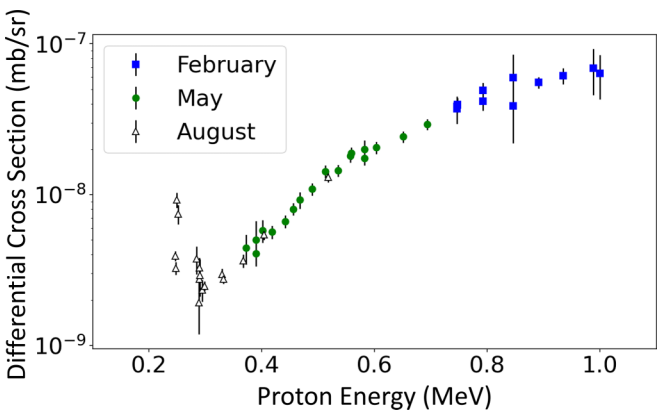

FIG. 7. Differential cross section for the R/DC → 6.79 MeV transition. Different measurement campaigns are indicated by the different symbols.

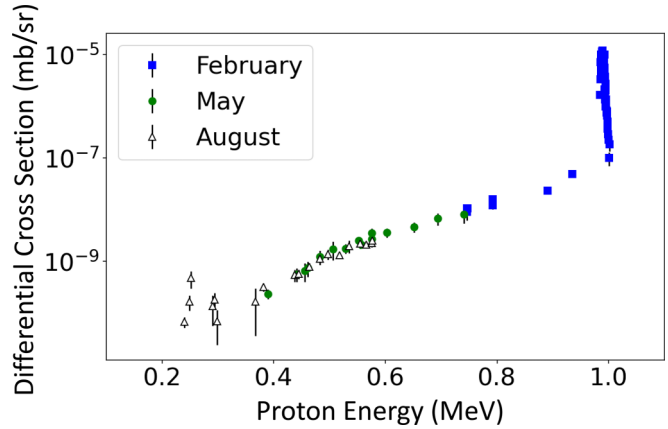

FIG. 8. As Fig. 7, but for the transition to the ground state.

6.79 MeV primary capture transitions, and the ^{14}N$(p,p)^{14}$N differential scattering cross-section data of [41]. The alternative parametrization of Brune [42] has two main advantages, it eliminates the need for boundary conditions and the fit parameters correspond directly to physical level parameters. A channel radius of 5.5 fm was adopted for the present work, as in Refs. [3,20,21,23].

The main focus of this work is on the ground state transition, as that is where the greatest inconsistencies between different data sets, and between the data and the R-matrix fit, are present. Because of complications encountered in past analyses [20,41], which will be discussed further in Sec. V, only the point-to-point uncertainties were included in the current fitting, that is, the systematic uncertainties were ignored. This is not usually good practice, but in this case, to better understand the model uncertainties, it was found to be a useful approach. The reason for this is that the systematic uncertainties of the data are relatively small compared to the model uncertainties since all of the data are normalized to the strength of the well known resonance at 278 keV. This resonance has a strength with an overall uncertainty of 2.4% and, for the ground state transition, an uncertainty in the branching ratio of 2%. Further, past measurements of the strength of the 278 keV resonance and its branching ratios are consistent (see Daigle *et al.* [22]), unlike the off-resonance data.

In past R-matrix fits of the ground state transition by Li *et al.* [20] and deBoer *et al.* [41], where the normalization uncertainties were allowed to vary, albeit constrained using the χ^2 function of those works, the best fits resulted in very large normalization factors >10% from the nominal value. These factors were much larger than the estimated few percent systematic uncertainties quoted for the majority of the experimental studies. As will be discussed further in Sec. V, this was due to the discrepancy between the R-matrix model and the data both on the high-energy side of the 278 keV resonance, between ≈300 and 500 keV, and on the low energy side, extending down to the lowest energy measurements.

For the ground state ^{14}N$(p,\gamma_0)^{15}$O reaction, the R-matrix fit is quite complicated at low energies since there are several components to the cross section: broad $3/2^+$ resonances, the low energy 278 keV resonance, background contributions

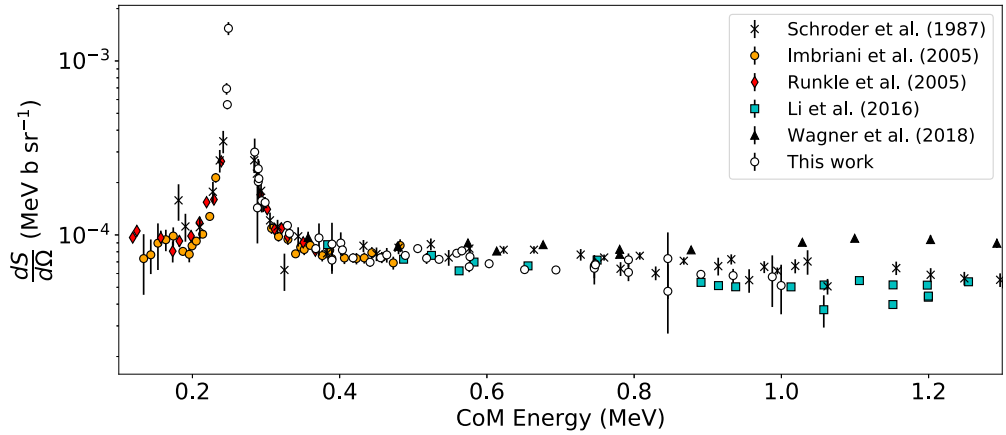

FIG. 9. S factors for the R/DC $\rightarrow$ 6.79 MeV transition for this work compared with those from Refs. [9,11–15,17,20,21,39]. The data series labeled LUNA represents the measurements of Refs. [11,14,17,39]. The data from this work and Li *et al.* [20] have been scaled by a factor of 4π for the purposes of plotting and comparing to previous works only, the data were treated as differential in the calculations. The data from Schröder *et al.* [9] are corrected according to Adelberger *et al.* [3].

from high lying levels, direct capture, and subthreshold states (see Fig. 2 of deBoer *et al.* [41]). Thus the phenomenological model requires many different types of data to constrain all of the possible components.

The cross-section data utilized in the fitting were taken from measurements at LUNA [11,14,17,39], LENA [15], Bochum [9], the University of Notre Dame [20,41], and Dresden [21]. Due to target effects, some of the data on the high energy side of narrow resonances were excluded. Corresponding to this, some of the parameters for narrow resonances were fixed to previously determined values as indicated in Table IV.

Through the fitting process, it was tested whether it was most appropriate to treat the various data sets for the ground state transition as angle integrated or differential cross sections. For the 6.79 MeV transition, the underlying angular distribution is well known, since the off-resonance cross section is dominated by direct capture (see Li *et al.* [20]). For the 6.17 MeV transition, the uncertainties in the present data are likely too large for these effects to be significant. For most of the prior data, the fitting was insensitive to this choice. However, by treating the ground state transition data of Schröder *et al.* [9] as differential cross sections, the results were dramatically improved, especially in the higher energy regions. Thus, the best fit from the data considered the present measurement, Schröder *et al.* [9], and Li *et al.* [20] as differential cross sections. The other data sets were also treated as differential cross sections, but no significant difference in fit quality was achieved over treating them as angle integrated. The resulting fits to the ground state transition are shown in Figs. 11 and 12 and the fit to the ^{14}N$(p, p)^{14}$N data in Fig. 13. The final fit parameters are given in Table IV.

For the low-energy contribution from the capture to the excited state at 6.79 MeV, the present data and fit are in good agreement with earlier investigations. The present extrapolated S factor for this transition is $S_{6.79}(0) = 1.24 \pm 0.09$ keV b. This agrees with the recent analysis of Wagner *et al.* [21] and lies between those reported by Adelberger *et al.* [3] and Li *et al.* [20], while agreeing with both within their quoted uncertainties. However, it should be noted that at proton energies above 700 keV we could not confirm the enhancement in the cross section that the authors reported in Wagner *et al.* [21].

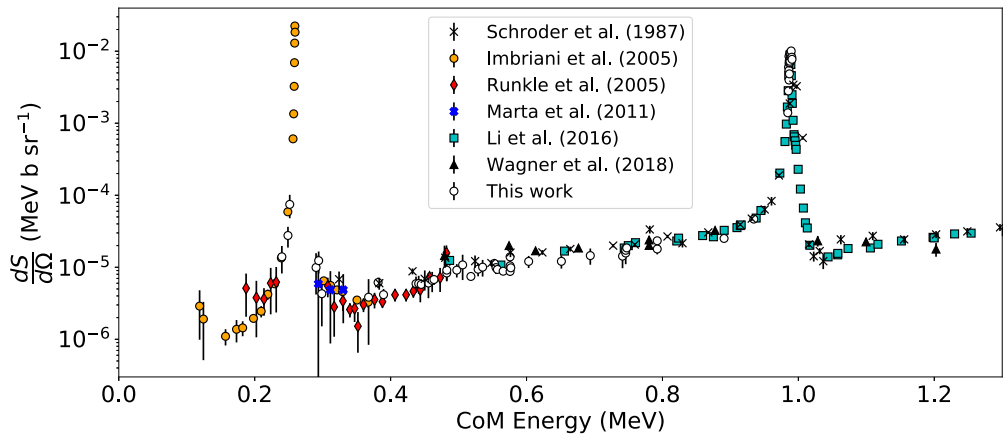

FIG. 10. As Fig. 9, but for the ground state transition.

TABLE IV. Levels used in the *R*-matrix fits. Bold values indicate parameters that were allowed to vary during the fit. The signs of the partial widths and ANCs indicate the signs of the corresponding reduced width amplitudes. The dividing line demarcates the proton separation energy at $E_x = 7.2968(5)$ MeV [34].

E_x (Refs. [22,34])	E_x (fit)	J^π	Channel	l	s	ANC (fm$^{-1/2}$) / Partial width (eV)
0.0	0.0	$1/2^-$	^{14}N+p	1	1/2	0.23
			^{14}N+p	1	3/2	7.4
6.7931(17)	6.7931	$3/2^+$	^{14}N+p	0	3/2	4.75
			^{15}O+$\gamma_{0.00}$	$E1$	1/2	**2.50**
7.5565(4)	7.5563	$1/2^+$	^{14}N+p	0	1/2	1.0×10^3
			^{15}O+$\gamma_{0.00}$	$E1$	1/2	$\mathbf{0.61 \times 10^{-4}}$
			^{15}O+$\gamma_{6.79}$	$M1$	3/2	8.22×10^{-3}
8.2840(5)	**8.2848**	$3/2^+$	^{14}N+p	2	1/2	**−92.2**
			^{14}N+p	0	3/2	$\mathbf{4.013 \times 10^3}$
			^{14}N+p	2	3/2	**−509**
			^{15}O+$\gamma_{0.00}$	$E1$	1/2	**0.244**
8.9821(17)	8.98	$5/2^-$	^{14}N+p	1	3/2	-5.872×10^3
			^{15}O+$\gamma_{0.00}$	$E2$	1/2	−0.303
			^{15}O+$\gamma_{6.79}$	$E1$	3/2	−0.001
9.484(8)	**9.488**	$3/2^+$	^{14}N+p	2	1/2	$\mathbf{77.69 \times 10^3}$
			^{14}N+p	0	3/2	$\mathbf{126.685 \times 10^3}$
			^{14}N+p	2	3/2	$\mathbf{-7.822 \times 10^3}$
			^{15}O+$\gamma_{0.00}$	$E1$	1/2	**6.92**
			^{15}O+$\gamma_{6.86}$	$M1$	5/2	0.2
9.488(3)	9.4905	$5/2^-$	^{14}N+p	3	1/2	$\mathbf{0.979 \times 10^3}$
			^{14}N+p	1	3/2	-6.576×10^3
			^{14}N+p	3	3/2	-0.985×10^3
			^{15}O+$\gamma_{0.00}$	$E2$	1/2	−0.307
			^{15}O+$\gamma_{6.79}$	$E1$	3/2	−0.0123
	15	$1/2^+$	^{14}N+p	0	3/2	4.0×10^6
			^{15}O+$\gamma_{0.00}$	$E1$	1/2	$\mathbf{1.0 \times 10^3}$
	15	$3/2^+$	^{14}N+p	0	3/2	4.722×10^6
			^{15}O+$\gamma_{0.00}$	E1	1/2	**327.3**

For the capture to the ground state, the best fit is similar to those obtained previously in Li *et al.* [20] and deBoer *et al.* [41], consistent with the discrepancies found in those works between the data and the *R*-matrix fit at low energies. These issues will be discussed further in Sec. V. The present result for the zero-energy extrapolated *S* factor is $S_{\mathrm{g.s.}}(0) = 0.33^{+0.16}_{-0.08}$ keV b. This value is higher than either that of Wagner *et al.* [21] (0.19 ± 0.05 keV b), Adelberger *et al.* [3] (0.27 ± 0.05 keV b), or Imbriani *et al.* [11] (0.25 ± 0.06 keV b) while being lower than that reported by

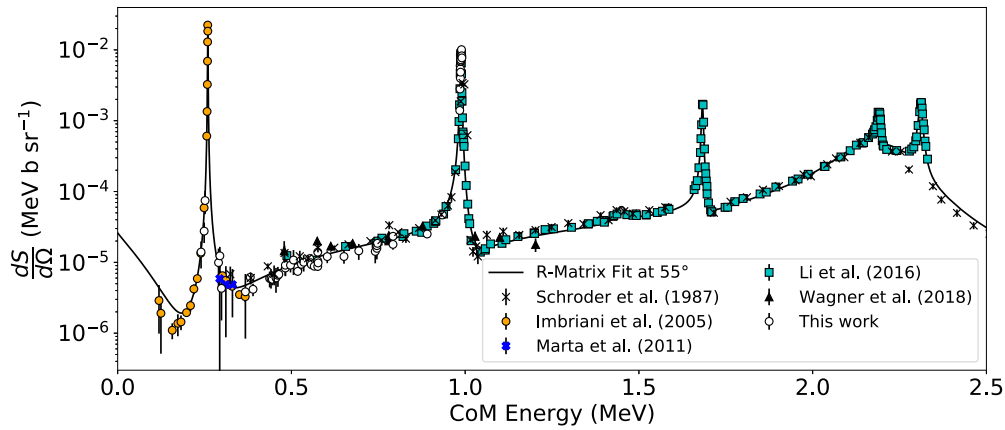

FIG. 11. Differential *S* factors for the R/DC → ground state transition for this work compared with Refs. [9,11,15,20,21,39] and the extrapolated differential *S*-factor curves calculated with the AZURE2 code. The data from Refs. [11,15,21,39] were originally reported as angle integrated, we have however converted them to differential ones in performing the fits. The data from Schröder *et al.* [9] are corrected according to Adelberger *et al.* [3] and then treated as differential cross sections (more detail in text).

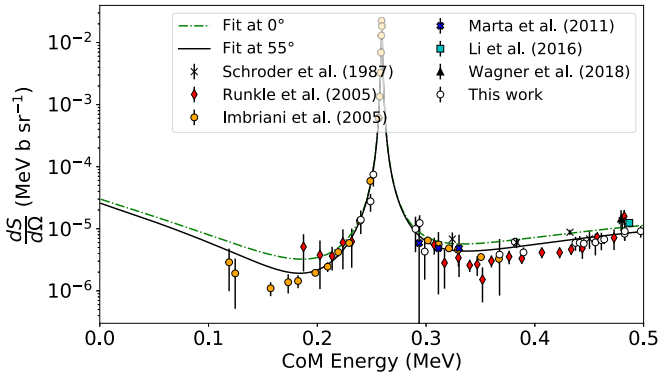

FIG. 12. As Fig. 11, but focusing on the low energy range of the S factor. Differential S factors for the R/DC → ground state transition from Runkle *et al.* [15] and Imbriani *et al.* [11], alongside the differential S factors determined in this work at 0° and 55°, respectively. The fits show significant differences in the behavior of the reaction below the resonance, where the large discrepancy between these data sets lie.

Li *et al.* [20] $[0.42 \pm 0.04(\text{stat})^{+0.09}_{-0.19}(\text{syst})$ keV b] and Runkle *et al.* [15] $(0.49 \pm 0.08$ keV b). With these results for context, the current extrapolated value lies in the middle of the landscape of previous extrapolations. However, it should be stressed that because of the poor reproduction of the low energy experimental data by the R-matrix fit, especially that of Imbriani *et al.* [11], the uncertainty in the extrapolation of the S factor is dominated by the systematic difference between data and model (see Fig. 12).

While the present study does not report any measurements for the transition to the excited state at 6.17 MeV, a fit was performed, and an S-factor extrapolation was made, using the data from Schröder *et al.* [9], Runkle *et al.* [15], and Imbriani *et al.* [11]. The present extrapolated S factor for this transition is $S_{6.17}(0) = 0.12 \pm 0.04$ keV b. This agrees well with the recently reported values of 0.12 given in Azuma *et al.* [19] and 0.13 ± 0.06 in Adelberger *et al.* [3].

With the above considerations, a total S factor for the $^{14}\text{N}(p,\gamma)^{15}\text{O}$ reaction was calculated, giving $S_{tot}(0) = 1.69 \pm 0.13$ keV b. This value, as well as those for the individual transitions, are compared to literature values in Table I. The other transitions, not explicitly reported in this section, are expected to contribute less than ≈5% to the total low energy S factor [3].

This total S factor, at zero-energy, is higher than those values reported in Refs. [3,11,14] but agrees reasonably well within uncertainty and is very close to the extrapolations reported in Refs. [15,18]. This analysis continues to suggests a higher low-energy S factor for the $^{14}\text{N}(p,\gamma)^{15}\text{O}$ reaction than suggested by the very low energy data of Imbriani *et al.* [11].

V. DISCUSSION

While the $^{14}\text{N}(p,\gamma)^{15}\text{O}$ reaction is one of the most important for modeling the CNO cycle, there are surprisingly few measurements and there are significant discrepancies between them over some important energy ranges. In particular, measurements of the ground state transition have shown the largest deviations, likely resulting from the small cross section and the large summing corrections that need to be applied to the yield data to reach an absolute cross section determination. The inconsistencies are most pronounced on the high energy side of the $E_p = 278$ keV resonance. Several measurements have been made over this region [9,11,15,20,21,39]. Much of

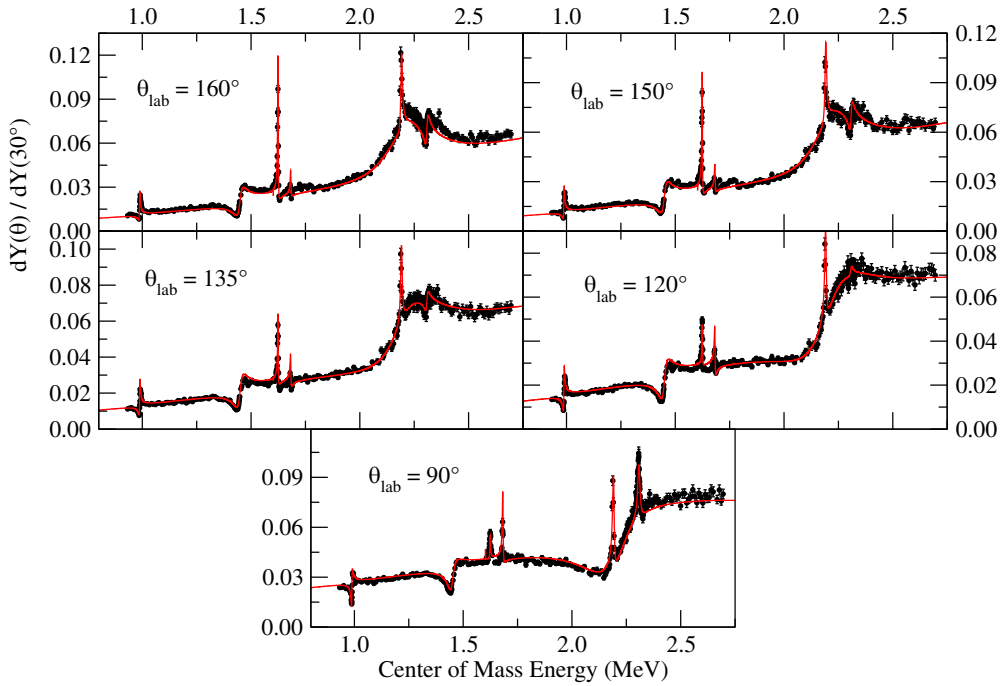

FIG. 13. R-matrix fit to the $^{14}\text{N}(p,p)^{14}\text{N}$ gas target data of [41] fit simultaneously with the $^{14}\text{N}(p,\gamma)^{15}\text{O}$ data discussed in the text.

the discrepant data may be the result of uncorrected target effects in the experimental yields. In particular, the well known issue of small amounts of target material diffusing into the backing, which affects the data directly above resonances (in this case the $E_p = 300$–500 keV range).

As can be seen in Figs. 11 and 12, the present data agree well with the data of Imbriani *et al.* [11] above the resonance at 278 keV, but the *R*-matrix simulations for this transition show a systematic deviation in the *S* factor below 450 keV center of mass energy. This suggests that an additional reaction component, not included in the phenomenological *R*-matrix description affects the low energy *S* factor of the transition.

Complicating the issue further, almost no reported *R*-matrix fit has been able to reproduce the low cross section data in the energy region from ≈300 to 500 keV [3,11,16,19–21], with only that of Runkle *et al.* [15] reporting good agreement. The issue is further exacerbated by problems in fitting the low energy data of Imbriani *et al.* [11] simultaneously with the higher energy data [20]. Thus, the inability to resolve the data and *R*-matrix fit discrepancies for the ground state transition results in the dominant source of uncertainty for the extrapolated low-energy *S* factor for the ground state transition and is therefore one of the largest uncertainty contributions remaining in the total capture cross section.

Several different options were explored in an effort to find the source of the discrepancy between the experimental data and the *R*-matrix fit above and below the 278 keV resonance. As the current *R*-matrix fits are unable to reproduce the interference pattern observed around the 278 keV resonance, calculations were made to see if other states could be added in the nearby energy range. While levels may have negligible branchings to different final states in the capture channels, possibly being too weak to be observed in some channels, all levels with a significant proton width must be consistent with the ^{14}N$(p,p)^{14}$N data.

Insight into possible missing levels in ^{15}O can be gained from the study of the mirror state ^{15}N, as recently reported by Mertin *et al.* [43]. Most significant for this study, the mirror of the $E_x = 9.152$ MeV, $3/2^-$ state in ^{15}N does not correspond to any observed level in ^{15}O. This level is expected to be at $E_x \approx 8.9$ MeV, which would correspond to a resonance in ^{14}N $+p$ reactions at $E_p \approx 1.7$ MeV. While this level is somewhat higher in energy, it could provide an additional source of interference if it is a broad resonance.

Calculations were made to test if a level of any spin up to $9/2$, which had a significant width ($\Gamma > 10$ keV), could be consistent with the available data between ≈300 and ≈600 keV. With the constraint of the scattering data, no viable solution could be found. However, at lower energies, where scattering data do not exist and where the Coulomb component of the scattering cross section would likely mask any nuclear contributions, the data could not rule out such a state.

The $E_x = 6.79$ MeV subthreshold state is thought to make a strong contribution to the low energy cross section of the ground state transition reaction, but other subthreshold states could also contribute, to a lesser, but still significant extent. The main candidate is the $E_x = 6.17$ MeV state. While the ANCs of both of the levels are well known [16,44], the ground state γ-ray width has only lower limits established from lifetime measurements (see Table II of Frentz *et al.* [23], for example) of about 0.5 eV. Assuming an $M1$ multipolarity and using the recommended upper limit (RUL) of 10 W.u. [45], gives an upper limit for the γ-ray width of approximately 50 eV.

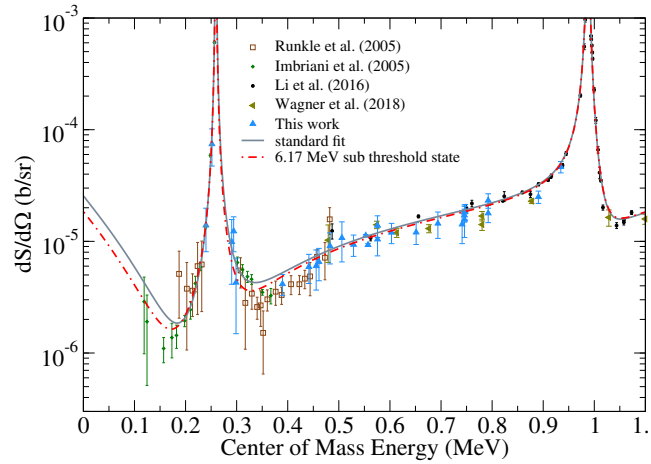

FIG. 14. *R*-matrix fit of the ^{14}N$(p,\gamma_0)^{15}$O data with an additional component for the 6.17 MeV subthreshold state.

An *R*-matrix fit that includes the $E_x = 6.17$ MeV state as a subthreshold contribution to the ground state transition is shown in Fig. 14 compared to the standard fit that does not include it. In this case, the fit resulted in a γ width of ≈6 eV, well within the range estimated above. While its inclusion does not completely resolve the discrepancy between the fit and the data, it shows that the 6.17 MeV level can make a significant contribution to the low energy cross section, and should not be ignored.

The reason for the differences in the *S* factor for the ^{14}N$(p,\gamma)^{15}$O ground state transition at very low energy between the direct measurement of Imbriani *et al.* [11] and the *R*-matrix extrapolation of the higher energy data cannot be explained at the present time and is therefore treated as a systematic uncertainty. In this energy region, the data sets of Imbriani *et al.* [11] and Runkle *et al.* [15] exhibit opposite behavior above and below the resonance. While reported as angle integrated, Imbriani *et al.* [11] and Runkle *et al.* [15] measured the reaction at 55° and 0° respectively, albeit, in very close geometry, and, as can be seen in Fig. 12, the discrepancy between the two is even more pronounced when treating the data as differential. These results indicate that there could be lingering angular effects causing the differences in this energy region.

In addition, Imbriani *et al.* [11] made some assumptions in their conversion from yield to *S* factors that could have additional unrealized uncertainties. For example, they state that all of the primary and secondary angular distributions they measured were isotropic within uncertainty (except for the primary transition to the 6.79 MeV state), and that these results were consistent with that of Schröder *et al.* [9], yet the angular distribution coefficients reported by Schröder *et al.*

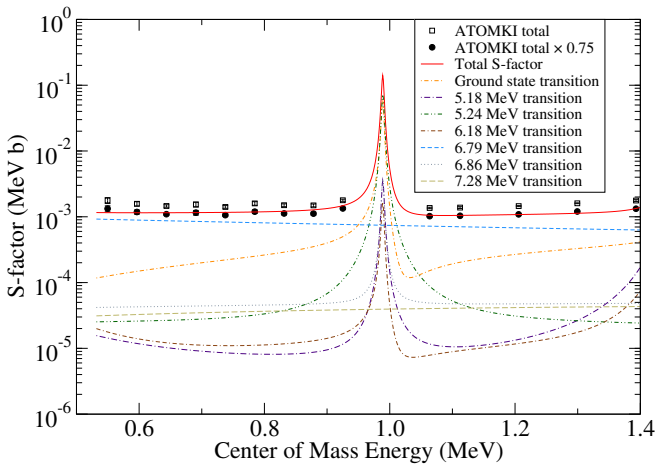

FIG. 15. Comparison of the sum of the partial *R*-matrix cross sections, from a global fit to past individual transition measurements, for all measured transitions compared to the total cross section data of Gyürky *et al.* [46]. While there is good agreement in the energy dependence of the fit and the data, the absolute scale of the *R*-matrix fit is undershoots the data by ≈25%. Both the scaled (black circles) and unscaled (black open squares) data of Gyürky *et al.* [46] are shown for comparison.

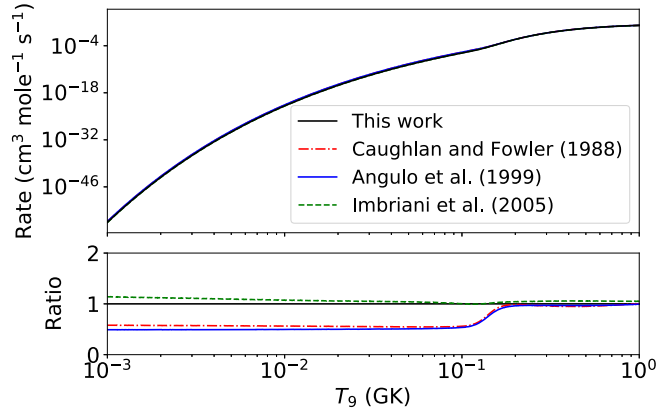

FIG. 16. The reaction rate from the present work compared with the rates presented in Caughlan and Fowler [48], Angulo *et al.* [49], and Imbriani *et al.* [11]. The rates in this work were calculated numerically with the AZURE2 code. It is important to note that the rates given in [48,49] were calculated solely from the uncorrected data of [9]. a) Reaction rates given in cm^3 mole^{-1} s^{-1}. b) Ratio of the present rate to the given literature rates.

[9], albeit at somewhat higher energies, indicate a measurable anisotropy in the ground state transition. Further, the thick target line shape analysis used by Imbriani *et al.* [11] may have unrealized uncertainty contributions, as the precise line shapes must be known. However, these line shapes can change shape as a function of target stoichiometry, which can change through out the experiment. It should be a top priority to remeasure the low energy range range only so far accessed by LUNA using a standard thin target or a gas jet target. Finally, the angular distributions measured by Li *et al.* [20] and Schröder *et al.* [9] only went down to approximately $E_p =$ 500 keV, and, as such, another investigation of the $^{14}\mathrm{N}(p,\gamma)^{15}\mathrm{O}$ reaction's angular distributions at these low energies is warranted.

Finally, recent activation measurements by Gyürky *et al.* [46] show a discrepancy between the total capture cross section measured via the activation technique, and that determined by taking the sum of the partial capture cross sections. While the energy dependence is in reasonably good agreement with fits like those from the present work, the absolute cross section is ≈25% larger than that determined from the *R*-matrix fit as shown in Fig. 15. Over the energy range of measurement, the 6.79 MeV and ground state transition data make up most of the total *S* factor, however, the *R*-matrix fit for several transitions is based solely on the experimental capture data of Schröder *et al.* [9], which has an estimated systematic uncertainty of ≈13%, and the direct contributions from the squared ANCs reported by Mukhamedzhanov *et al.* [16], which have uncertainties of ≈10%. Considering these estimated uncertainties, the 25% difference between the fit and the data of Gyürky *et al.* [46] is quite significant, as the systematic uncertainty of that work is estimated to be considerably smaller, ≈7%. This disagreement is further indication that the modeling or interpretation of the present $^{14}\mathrm{N}(p,\gamma)^{15}\mathrm{O}$ data remains incomplete and further study, especially of those transitions only observed in this energy range by Schröder *et al.* [9], are needed.

VI. REACTION RATES

For the transitions reported here, the reaction rates were calculated by numerical integration of the cross sections with the AZURE2 code for the temperature range of 0.001 GK to 10 GK with 2000 steps spaced equally in $\log(T)$ (see the Supplemental Material [38]) using

$$N_A\langle\sigma v\rangle = \left(\frac{8}{\pi\mu}\right)^{1/2}\frac{N_A}{(k_BT)^{3/2}}\int_0^\infty \sigma(E)Ee^{-E/k_BT}dE, \quad (6)$$

where μ is the reduced mass, $E = \mu v^2/2$ is the center-of-mass energy, N_A is Avogadro's number, and k_B is Boltzmann's constant.

The reaction rate contributions from the ground state and 6.79 MeV transitions were calculated from the *R*-matrix fit described in Sec. IV and thus were determined from the present data in tandem with the literature data of Refs. [9,11,14,15,17,20,21,39], while the contribution from the 6.17 MeV transition were determined from the literature data of Refs. [9,11,15]. Finally, the remainder of the strength for the $E_x = 7.556$ MeV level (278 keV resonance) from other transitions was added to the reaction rate using the narrow resonance approximation [47] and the branching information presented in Daigle *et al.* [22].

The results for the reaction rates are compared with those from Caughlan and Fowler [48], Angulo *et al.* [49], and Imbriani *et al.* [11] in Fig. 16. At lower temperatures, the present rate is approximately 15% higher than those published by Imbriani *et al.* [11], while the present rates are lower than the other two reported values. It should be considered that the calculations of Caughlan and Fowler [48] and Angulo *et al.*

[49] are based only on the uncorrected data from Schröder *et al.* [9]. Ultimately, the present higher zero-energy S factors translate into a higher reaction rate at stellar temperatures, indicating a better agreement with the results presented by the Borexino group [30].

VII. SUMMARY AND CONCLUSIONS

New cross sections of the ^{14}N$(p,\gamma)^{15}$O reaction have been measured from $E_p = 0.27$ to 1.07 MeV for the ground state and 6.79 MeV transitions at the CASPAR facility. These measurements bridge the gap between low-energy measurements of Refs. [11,14,15,17,39] and those at high energy [9,20]. R-matrix fits were performed in order to extrapolate into the astrophysically relevant energy region.

A comprehensive multichannel R-matrix analysis was performed simultaneously for both the transition to the ground state, the excited states at $E_x = 6.17$ and 6.79 MeV, as well as ^{14}N$(p,p)^{14}$N differential scattering data. Incorporating recent results for the lifetime of the excited state at 6.79 MeV [23], the present study finds the extrapolated zero-energy S-factor components for each of the two transitions to be $S_{\text{g.s.}}(0) = 0.33^{+0.16}_{-0.08}$ keV b and $S_{6.79}(0) = 1.24 \pm 0.09$ keV b. These reported uncertainties reflect the fact that there are clear, systematic differences between the measured low-energy data of Imbriani *et al.* [11] and Runkle *et al.* [15] that are not being effectively captured in the R-matrix fit.

Through the R-matrix fits, it was found that it was more appropriate to treat the corrected data from Schröder *et al.* [9] as differential cross sections instead of angle integrated. Ultimately, the present data agreed well with those of [9,11,15,20,21,39] across the energy range in question for both transitions, with the notable exception that the enhancement in the 6.79 MeV transition seen in Wagner *et al.* [21] could not be confirmed here.

This new S factor translates into a change of the reaction rate, with the new rate approximately 50% smaller than that given in previous tabulations such as Caughlan and Fowler [48] and Angulo *et al.* [49] and 15% larger than those based on the LUNA predictions [11]. During CNO burning, the various associated nuclear processes are in equilibrium [50], and the increased rate would, therefore, translate into an increase in the CNO neutrino production from the decay of ^{15}O, because the solar ^{15}O decay rate corresponds directly to the ^{14}N$(p,\gamma)^{15}$O production rate. This result, in principle, supports the increased neutrino flux reported by the Borexino Group [30]. A formal comparison is beyond the scope of this paper, however, since the details of the Borexino measurement and the associated corrections for neutrino oscillations have not yet been published.

After the recent measurement providing the most stringent constraint of the lifetime of the 6.79 MeV state [23] and this work, it can be broadly concluded that the largest sources of uncertainty within this reaction now lies in the weaker transitions, specifically at low energies. Additional measurements of the ground-state transition at low energies could yield further insights, particularly with angular distribution measurements at energies below those performed by Li *et al.* [20] and additional measurements below the 278 keV resonance. To have a significant impact, however, would likely require concentrated, extended counting times due to the extremely low rates at the energies of interest, which would be ideally suited for the CASPAR [31], LUNA [51], or the newly installed JUNA facilities [52].

ACKNOWLEDGMENTS

We are indebted to Harald Leiste (Institute for Applied Materials, KIT) and the Karlsruhe Nano Micro Facility at the Karlsruhe Institute of Technology for the production of the ZrN targets. Figure 1 has been created using the SciDraw scientific figure preparation system [53]. This research utilized resources from the Notre Dame Center for Research Computing and was funded by the National Science Foundation through Grant No. PHY-2011890 (University of Notre Dame Nuclear Science Laboratory), Grant No. PHY-1430152 (the Joint Institute for Nuclear Astrophysics - Center for the Evolution of the Elements), Grant No. PHY-1615197 (The Compact Accelerator System for Performing Astrophysical Research at the Sanford Underground Research Facility), and the U.S. Department of Energy's (DOE) National Nuclear Security Administration (NNSA, Grant No. DE-NA0003888) and the Sanford Underground Research Facility (SURF, Grant No. DE-SC0020216).

[1] J. N. Bahcall, S. Basu, M. Pinsonneault, and A. M. Serenelli, Helioseismological implications of recent solar abundance determinations, Astrophys. J. **618**, 1049 (2005).

[2] A. B. McDonald, Solar neutrinos, New J. Phys. **6**, 121 (2004).

[3] E. Adelberger, A. García, R. Hamish Robertson, K. Snover, A. Balantekin, K. M. Heeger, M. Ramsey-Musolf, D. Bemmerer, A. Junghans, C. A. Bertulani, J.-W. Chen, H. Costantini, P. Prati, M. Couder, E. Uberseder, M. Wiescher, R. Cyburt, B. Davids, S. J. Freedman, M. Gai, D. Gazit, L. Gialanella, G. Imbriani, U. Greife, M. Hass, W. C. Haxton, T. Itahashi, K. Kubodera, K. Langanke, D. Leitner, M. Leitner, P. Vetter, L. Winslow, L. Marcucci, T. Motobayashi, A. Mukhamedzhanov, R. E. Tribble, K. M. Nollett, F. M. Nunes, T.-S. Park, P. Parker, R. Schiavilla, E. C. Simpson, C. Spitaleri, F. Strieder, H.-P. Trautvetter, K. Suemmerer, and S. Typel, Solar fusion cross sections. II. The pp chain and CNO cycles, Rev. Mod. Phys. **83**, 195 (2011).

[4] H. A. Bethe, Energy Production in stars, Phys. Rev. **55**, 434 (1939).

[5] J. N. Bahcall and M. H. Pinsonneault, What Do We (Not) Know Theoretically about Solar Neutrino Fluxes? Phys. Rev. Lett. **92**, 121301 (2004).

[6] J. N. Bahcall, A. M. Serenelli, and S. Basu, 10,000 standard solar models: A Monte Carlo simulation, Astrophys. J. Suppl. Series **165**, 400 (2006).

[7] M. Asplund, N. Grevesse, and A. Jacques Sauval, The solar chemical composition, Nucl. Phys. A **777**, 1 (2006), special Issue on Nuclear Astrophysics.

[8] W. C. Haxton and A. M. Serenelli, CN cycle solar neutrinos and the sun's primordial core metallicity, Astrophys. J. **687**, 678 (2008).

[9] U. Schröder, H. Becker, G. Bogaert, J. Görres, C. Rolfs, H. P. Trautvetter, R. Azuma, C. Campbell, J. King, and J. Vise, Stellar reaction rate of ^{14}N$(p,\gamma)^{15}$O and hydrogen burning in massive stars, Nucl. Phys. A **467**, 240 (1987).

[10] C. Angulo and P. Descouvemont, The ^{14}N$(p,\gamma)^{15}$O low-energy S-factor, Nucl. Phys. A **690**, 755 (2001).

[11] G. Imbriani, H. Costantini, A. Formicola, A. Vomiero, C. Angulo, D. Bemmerer, R. Bonetti, C. Broggini, F. Confortola, P. Corvisiero, J. Cruz, P. Descouvemont, Z. Fülöp, G. Gervino, A. Guglielmetti, C. Gustavino, G. Gyürky, A. P. Jesus, M. Junker, J. N. Klug, A. Lemut, R. Menegazzo, P. Prati, V. Roca, C. Rolfs, M. Romano, C. Rossi-Alvarez, F. Schümann, D. Schürmann, E. Somorjai, O. Straniero, F. Strieder, F. Terrasi, and H. P. Trautvetter, S-factor of ^{14}N$(p,\gamma)^{15}$O at astrophysical energies, Eur. Phys. J. A **25**, 455 (2005).

[12] A. Lemut, D. Bemmerer, F. Confortola, R. Bonetti, C. Broggini, P. Corvisiero, H. Costantini, J. Cruz, A. Formicola, Z. Fülöp, G. Gervino, A. Guglielmetti, C. Gustavino, G. Gyürky, G. Imbriani, A. P. Jesus, M. Junker, B. Limata, R. Menegazzo, P. Prati, V. Roca, D. Rogalla, C. Rolfs, M. Romano, C. Rossi Alvarez, F. Schümann, E. Somorjai, O. Straniero, F. Strieder, F. Terrasi, and H. P. Trautvetter, First measurement of the ^{14}N$(p,\gamma)^{15}$O cross section down to 70 keV, Phys. Lett. B **634**, 483 (2006).

[13] D. Bemmerer, F. Confortola, A. Lemut, R. Bonetti, C. Broggini, P. Corvisiero, H. Costantini, J. Cruz, A. Formicola, Z. Fülöp, G. Gervino, A. Guglielmetti, C. Gustavino, G. Gyürky, G. Imbriani, A. Jesus, M. Junker, B. Limata, R. Menegazzo, P. Prati, V. Roca, C. Rolfs, D. Rogalla, M. Romano, C. Rossi-Alvarez, F. Schümann, E. Somorjai, O. Straniero, F. Strieder, F. Terrasi, and H. P. Trautvetter, Low energy measurement of the ^{14}N$(p,\gamma)^{15}$O total cross section at the LUNA underground facility, Nucl. Phys. A **779**, 297 (2006).

[14] M. Marta, A. Formicola, G. Gyürky, D. Bemmerer, C. Broggini, A. Caciolli, P. Corvisiero, H. Costantini, Z. Elekes, Z. Fülöp, G. Gervino, A. Guglielmetti, C. Gustavino, G. Imbriani, M. Junker, R. Kunz, A. Lemut, B. Limata, C. Mazzocchi, R. Menegazzo, P. Prati, V. Roca, C. Rolfs, M. Romano, C. R. Alvarez, E. Somorjai, O. Straniero, F. Strieder, F. Terrasi, H. P. Trautvetter, and A. Vomiero, Precision study of ground state capture in the ^{14}N$(p,\gamma)^{15}$O reaction, Phys. Rev. C **78**, 022802 (2008).

[15] R. C. Runkle, A. E. Champagne, C. Angulo, C. Fox, C. Iliadis, R. Longland, and J. Pollanen, Direct Measurement of the ^{14}N$(p,\gamma)^{15}$O S Factor, Phys. Rev. Lett. **94**, 082503 (2005).

[16] A. M. Mukhamedzhanov, P. Bém, B. A. Brown, V. Burjan, C. A. Gagliardi, V. Kroha, J. Novák, F. M. Nunes, Š. Piskoř, F. Pirlepesov, E. Šimečková, R. E. Tribble, and J. Vincour, Asymptotic normalization coefficients for ^{14}N + p $\rightarrow$ ^{15}O and the astrophysical S factor for ^{14}N(p, γ)^{15}O, Phys. Rev. C **67**, 065804 (2003).

[17] A. Formicola, G. Imbriani, H. Costantini, C. Angulo, D. Bemmerer, R. Bonetti, C. Broggini, P. Corvisiero, J. Cruz, P. Descouvemont, Z. Fülöp, G. Gervino, A. Guglielmetti, C. Gustavino, G. Gyürky, A. P. Jesus, M. Junker, A. Lemut, R. Menegazzo, P. Prati, V. Roca, C. Rolfs, M. Romano, C. Rossi Alvarez, F. Schümann, E. Somorjai, O. Straniero, F. Strieder, F. Terrasi, H. P. Trautvetter, A. Vomiero, and S. Zavatarelli, Astrophysical S-factor of ^{14}N$(p,\gamma)^{15}$O, Phys. Lett. B **591**, 61 (2004).

[18] C. Angulo, A. E. Champagne, and H. P. Trautvetter, R-matrix analysis of the ^{14}N$(p,\gamma)^{15}$O astrophysical S-factor, Nucl. Phys. A **758**, 391 (2005).

[19] R. E. Azuma, E. Uberseder, E. C. Simpson, C. R. Brune, H. Costantini, R. J. De Boer, J. Görres, M. Heil, P. J. Leblanc, C. Ugalde, and M. Wiescher, AZURE: An R-matrix code for nuclear astrophysics, Phys. Rev. C **81**, 045805 (2010).

[20] Q. Li, J. Görres, R. J. deBoer, G. Imbriani, A. Best, A. Kontos, P. J. LeBlanc, E. Uberseder, and M. Wiescher, Cross section measurement of ^{14}N$(p,\gamma)^{15}$O in the CNO cycle, Phys. Rev. C **93**, 055806 (2016).

[21] L. Wagner, S. Akhmadaliev, M. Anders, D. Bemmerer, A. Caciolli, S. Gohl, M. Grieger, A. Junghans, M. Marta, F. Munnik, T. P. Reinhardt, S. Reinicke, M. Röder, K. Schmidt, R. Schwengner, M. Serfling, M. P. Takács, T. Szücs, A. Vomiero, A. Wagner, and K. Zuber, Astrophysical S factor of the ^{14}N$(p,\gamma)^{15}$O reaction at 0.4–1.3 MeV, Phys. Rev. C **97**, 015801 (2018).

[22] S. Daigle, K. J. Kelly, A. E. Champagne, M. Q. Buckner, C. Iliadis, and C. Howard, Measurement of the $E_{\text{c.m.}} = 259$ keV resonance in the ^{14}N$(p,\gamma)^{15}$O reaction, Phys. Rev. C **95**, 015806 (2016).

[23] B. Frentz, A. Aprahamian, A. M. Clark, R. J. Deboer, C. Dulal, J. D. Enright, J. Görres, S. L. Henderson, J. D. Hinnefeld, K. B. Howard, R. Kelmar, K. Lee, L. Morales, S. Moylan, Z. Rahman, W. Tan, L. E. Weghorn, and M. Wiescher, Lifetime measurements of excited states in ^{15}O, Phys. Rev. C **103**, 045802 (2021).

[24] P. F. Bertone, A. E. Champagne, D. C. Powell, C. Iliadis, S. E. Hale, and V. Y. Hansper, Lifetime of the 6793-keV State in ^{15}O, Phys. Rev. Lett. **87**, 152501 (2001).

[25] D. Schürmann, R. Kunz, I. Lingner, C. Rolfs, F. Schümann, F. Strieder, and H. P. Trautvetter, Lifetime measurement of the 6792 keV state in ^{15}O, important for the astrophysical S factor extrapolation in ^{14}N$(p,\gamma)^{15}$O, Phys. Rev. C **77**, 055803 (2008).

[26] K. Yamada, T. Motobayashi, H. Akiyoshi, N. Aoi, Z. Fülöp, T. Gomi, Y. Higurashi, N. Imai, N. Iwasa, H. Iwasaki, Y. Iwata, H. Kobayashi, M. Kurokawa, Z. Liu, T. Minemura, S. Ozawa, H. Sakurai, M. Serata, S. Shimoura, S. Takeuchi, T. Teranishi, Y. Yanagisawa, K. Yoshida, and M. Ishihara, E1 strength of the subthreshold $3/2^+$ state in ^{15}O studied by Coulomb excitation, Phys. Lett. B **579**, 265 (2004).

[27] N. Galinski, S. K. Sjue, G. C. Ball, D. S. Cross, B. Davids, H. Al Falou, A. B. Garnsworthy, G. Hackman, U. Hager, D. A. Howell, M. Jones, R. Kanungo, R. Kshetri, K. G. Leach, J. R. Leslie, M. Moukaddam, J. N. Orce, E. T. Rand, C. Ruiz, G. Ruprecht, M. A. Schumaker, C. E. Svensson, S. Triambak, and C. D. Unsworth, Lifetime measurements of states in ^{15}O, Phys. Rev. C **90**, 035803 (2014).

[28] C. Michelagnoli, The lifetime of the 6.79 MeV state in ^{15}O as a challenge for nuclear astrophysics and γ-ray spectroscopy: A new DSAM measurement with the AGATA Demonstrator array, Ph.D. thesis, Università degli Studi di Padova (2013).

[29] S. Sharma, A. Gupta, M. R. Chowdhury, A. Mandal, A. Bisoi, V. Nanal, L. C. Tribedi, and M. S. Sarkar, Proton capture resonant state of ^{15}O at 7556 keV, Phys. Rev. C **102**, 024308 (2020).

[30] Borexino Collaboration, K. Altenmüller, S. Appel, V. Atroshchenko, Z. Bagdasarian, D. Basilico, G. Bellini, J. Benziger, R. Biondi, D. Bravo, B. Caccianiga, F. Calaprice, A. Caminata, P. Cavalcante, A. Chepurnov, D. D'Angelo, S.

Davini, A. Derbin, A. Di Giacinto, V. Di Marcello, X. F. Ding, A. Di Ludovico, L. Di Noto, I. Drachnev, A. Formozov, D. Franco, C. Galbiati, C. Ghiano, M. Giammarchi, A. Goretti, A. S. Göttel, M. Gromov, D. Guffanti, A. Ianni, A. Ianni, A. Jany, D. Jeschke, V. Kobychev, G. Korga, S. Kumaran, M. Laubenstein, E. Litvinovich, P. Lombardi, I. Lomskaya, L. Ludhova, G. Lukyanchenko, L. Lukyanchenko, I. Machulin, J. Martyn, E. Meroni, M. Meyer, L. Miramonti, M. Misiaszek, V. Muratova, B. Neumair, M. Nieslony, R. Nugmanov, L. Oberauer, V. Orekhov, F. Ortica, M. Pallavicini, L. Papp, L. Pelicci, Penek, L. Pietrofaccia, N. Pilipenko, A. Pocar, G. Raikov, M. T. Ranalli, G. Ranucci, A. Razeto, A. Re, M. Redchuk, A. Romani, N. Rossi, S. Schönert, D. Semenov, G. Settanta, M. Skorokhvatov, A. Singhal, O. Smirnov, A. Sotnikov, Y. Suvorov, R. Tartaglia, G. Testera, J. Thurn, E. Unzhakov, F. L. Villante, A. Vishneva, R. B. Vogelaar, F. von Feilitzsch, M. Wojcik, M. Wurm, S. Zavatarelli, K. Zuber, and G. Zuzel, Experimental evidence of neutrinos produced in the CNO fusion cycle in the Sun, Nature (London) **587**, 577 (2020).

[31] D. Robertson, M. Couder, U. Greife, F. Strieder, and M. Wiescher, Underground nuclear astrophysics studies with CASPAR, EPJ Web Conf. **109**, 09002 (2016).

[32] J. Heise, The sanford underground research facility, J. Phys.: Conf. Ser. **2156**, 012172 (2021).

[33] A. Antilla, J. Keinonen, M. Hautala, and I. Forsblom, Use of the ^{27}Al$(p,\gamma)^{28}$Si, $E_p = 992$ keV resonance as a gamma-ray intensity standard, Nucl. Instrum. Methods **147**, 501 (1977).

[34] F. Ajzenberg-Selove, Energy levels of light nuclei A = 13-15, Nucl. Phys. A **523**, 1 (1991).

[35] G. F. Knoll, *Radiation Detection and Measurement*, 3rd ed. (John Wiley & Sons, Inc., New York, 2000).

[36] M. Blaauw and S. J. Gelsema, Cascade summing in gamma-ray spectrometry in Marinelli-Beaker geometries: The third efficiency curve, Nucl. Instrum. Methods Phys. Res. A **505**, 311 (2003).

[37] M. E. Rose, The analysis of angular correlation and angular distribution data, Phys. Rev. **91**, 610 (1953).

[38] See Supplemental Material at http://link.aps.org/supplemental/10.1103/PhysRevC.106.065803 for the experimental data and tabulated reaction rate.

[39] M. Marta, A. Formicola, D. Bemmerer, C. Broggini, A. Caciolli, P. Corvisiero, H. Costantini, Z. Elekes, Z. Fülöp, G. Gervino, A. Guglielmetti, C. Gustavino, G. Gyürky, G. Imbriani, M. Junker, A. Lemut, B. Limata, C. Mazzocchi, R. Menegazzo, P. Prati, V. Roca, C. Rolfs, C. Rossi Alvarez, E. Somorjai, O. Straniero, F. Strieder, F. Terrasi, H. P. Trautvetter, and A. Vomiero, The ^{14}N$(p,\gamma)^{15}$O reaction studied with a composite germanium detector, Phys. Rev. C **83**, 045804 (2011).

[40] E. Uberseder and R. J. deBoer, AZURE2 user manual (2015), https://azure.nd.edu.

[41] R. J. deBoer, D. W. Bardayan, J. Görres, P. J. LeBlanc, K. V. Manukyan, M. T. Moran, K. Smith, W. Tan, E. Uberseder, M. Wiescher, P. F. Bertone, A. E. Champagne, and M. S. Islam, Low energy scattering cross section ratios of ^{14}N$(p,p)^{14}$N, Phys. Rev. C **91**, 045804 (2015).

[42] C. R. Brune, Alternative parametrization of *R*-matrix theory, Phys. Rev. C **66**, 044611 (2002).

[43] C. E. Mertin, D. D. Caussyn, A. M. Crisp, N. Keeley, K. W. Kemper, O. Momotyuk, B. T. Roeder, and A. Volya, Single particle strengths and mirror states in ^{15}N $-^{15}$O below 12.0 MeV, Phys. Rev. C **91**, 044317 (2015).

[44] P. F. Bertone, A. E. Champagne, M. Boswell, C. Iliadis, S. E. Hale, V. Y. Hansper, and D. C. Powell, ^{14}N$(^3$He, $d)^{15}$O as a probe of direct capture in the ^{14}N$(p,\gamma)^{15}$O reaction, Phys. Rev. C **66**, 055804 (2002).

[45] P. Endt, Strengths of gamma-ray transitions in $A = 5$-44 nuclei, IV, At. Data Nucl. Data Tables **55**, 171 (1993).

[46] G. Gyürky, Z. Halász, G. G. Kiss, T. Szücs, and Z. Fülöp, Activation cross section measurement of the ^{14}N$(p,\gamma)^{15}$O astrophysical key reaction, Phys. Rev. C **105**, L022801 (2022).

[47] W. A. Fowler, C. C. Lauritsen, and T. Lauritsen, Gamma-radiation from excited states of light nuclei, Rev. Mod. Phys. **20**, 236 (1948).

[48] G. R. Caughlan and W. A. Fowler, Thermonuclear reaction rates V, At. Data Nucl. Data Tables **40**, 283 (1988).

[49] C. Angulo, M. Arnould, M. Rayet, P. Descouvemont, D. Baye, C. Leclercq-Willain, A. Coc, S. Barhoumi, P. Aguer, C. Rolfs, R. Kunz, J. Hammer, A. Mayer, T. Paradellis, S. Kossionides, C. Chronidou, K. Spyrou, S. Degl'Innocenti, G. Fiorentini, B. Ricci, S. Zavatarelli, C. Providencia, H. Wolters, J. Soares, C. Grama, J. Rahighi, A. Shotter, and M. Lamehi Rachti, A compilation of charged-particle induced thermonuclear reaction rates, Nucl. Phys. A **656**, 3 (1999).

[50] M. Wiescher, J. Görres, E. Uberseder, G. Imbriani, and M. Pignatari, The cold and hot CNO cycles, Annu. Rev. Nucl. Part. Sci. **60**, 381 (2010).

[51] A. Formicola, G. Imbriani, M. Junker, D. Bemmerer, R. Bonetti, C. Broggini, C. Casella, P. Corvisiero, H. Costantini, G. Gervino, C. Gustavino, A. Lemut, P. Prati, V. Roca, C. Rolfs, M. Romano, D. Schürmann, F. Strieder, F. Terrasi, H.-P. Trautvetter, and S. Zavatarelli, The LUNA II 400kV accelerator, Nucl. Instrum. Methods Phys. Res. A **507**, 609 (2003).

[52] W. Liu, Z. Li, and J. J. He (JUNA Collaboration), Progress of Jinping underground laboratory for nuclear astrophysics (JUNA), Sci. China Phys. Mech. Astron. **59**, 642001 (2016).

[53] M. A. Caprio, LevelScheme A level scheme drawing and scientific figure preparation system for Mathematica, Comput. Phys. Commun. **171**, 107 (2005); http://scidraw.nd.edu